

Article

Synthesis and Crystal Structure Analysis of Some Aromatic Imines of Syringaldehyde

Christopher G. Hamaker *  and Stephan M. Germann

Department of Chemistry, Illinois State University, Normal, IL 61790-4160, USA

* Correspondence: chamaker@illinoisstate.edu; Tel.: +1-309-438-7659

Abstract: A series of syringaldehyde imines with *para*-substituted anilines have been synthesized in a good yield, and their crystal structures have been analyzed. The orientation of the syringaldehyde hydroxyl group plays an important role in the intermolecular hydrogen-bonding pattern of the molecules. The O–H···N hydrogen bonding interactions primarily determine the three-dimensional packing of the molecules, even though they make up a relatively small percentage of intermolecular interactions in the molecules. The three structures with the *p*-hydroxy group *cis* to the imine group give hydrogen-bonded zigzag chains in the monoclinic crystals, while the structure with a *trans* hydroxy group crystallizes in a hexagonal space group ($R\bar{3}$) and forms hydrogen-bonded hexamers. The hexagonal structure also displays Br···Br interactions, forming additional hexameric clusters. The analysis of published *p*-hydroxyphenyl imine crystal structures from the Cambridge Crystallographic Database revealed patterns in the length of the hydrogen bonding interactions based on steric congestion around the hydroxyl group.

Keywords: concomitant polymorph; crystal structure; Schiff base; hydrogen bonding



Citation: Hamaker, C.G.; Germann, S.M. Synthesis and Crystal Structure Analysis of Some Aromatic Imines of Syringaldehyde. *Crystals* **2024**, *14*, 99. <https://doi.org/10.3390/cryst14010099>

Academic Editors: Lilianna Checinska and Magdalena Małacka

Received: 27 December 2023

Revised: 12 January 2024

Accepted: 14 January 2024

Published: 22 January 2024



Copyright: © 2024 by the authors. Licensee MDPI, Basel, Switzerland. This article is an open access article distributed under the terms and conditions of the Creative Commons Attribution (CC BY) license (<https://creativecommons.org/licenses/by/4.0/>).

1. Introduction

The German–Italian chemist, Hugo Schiff, developed a new class of organic compound in 1864, the imine, or Schiff base [1]. The synthesis of Schiff base compounds is simple; it is the condensation of an amine and a carbonyl to give a carbon–nitrogen double bond. The simplicity of this synthesis has led to the extensive study of imines because they can easily be synthesized and modified. This diverse chemistry has been used to prepare a wide variety of Schiff bases that can be used as ligands in metal complexes [2–5]. Hydroxy-substituted imine derivatives have been used as ligands for many transition metals. Recently, the catechol-derived Schiff base ligands of thiacalixarene have been shown to preferentially bind copper (II) ions and were subsequently used to prepare copper-containing organic–inorganic materials [6].

Syringaldehyde is an aromatic aldehyde that is found in spruce, maple, [7,8] and oak woods and is an important flavor component of whiskey [9,10]. Recently, syringaldehyde has been shown to have biological activity [11], including antihyperglycemic activity [12,13], antioxidant activity [14,15], and anti-inflammatory activity [16]. In fact, phenol-containing Schiff bases often show biological activity. In a recent report by Aytac et al., a series of Schiff base compounds with phenol rings were synthesized and shown to have not only antioxidant activity, but many were inhibitors of acetylcholinesterase, butylcholinesterase, and/or carbonic anhydrase [17].

A polymorph has been defined as “a solid crystalline phase of a given compound resulting from the possibility of at least two crystalline arrangements of the molecules of that compound in the solid state” [18]. Concomitant polymorphs are formed simultaneously in the same crystallization medium and are much less frequently studied [19]. Concomitant polymorphs are seen in a variety of molecules. Gong et al. found concomitant polymorphs for methoxyflavone, a non-steroidal anabolic isoflavone [20]. Jones and co-workers found

two concomitant polymorphs of a polyamide molecules, which differ in their hydrogen-bonding patterns in the crystal [21]. The existence of polymorphs is important in many industries, but especially in the pharmaceutical industry since different polymorphs will have different properties [22]. While many a scientist who has tried to predict crystal structures has been called a fool in the rain, by systematically studying the structures of related molecules, crystal structure prediction may someday become a reality.

Our group is interested in the synthesis and crystal structures of Schiff bases, sulfonamides, and related molecules [23–25]. As part of our ongoing studies, we report the synthesis, spectral properties, and crystal structures of three Schiff bases from the condensation of syringaldehyde with several *para*-substituted aniline derivatives, including two concomitant polymorphs of the bromo-substituted compound.

2. Materials and Methods

2.1. General Experimental

The reagents were of reagent grade or better and obtained from standard commercial sources. Melting points were collected using Mel-Temp equipment from Laboratory Devices Inc. (Auburn, CA, USA) and are uncorrected. Infrared spectra were obtained as solid samples using a Agilent Cary 630 FT-IR spectrometer equipped with a diamond stage automated total reflectance attachment. NMR spectra were collected as solutions in DMSO- d_6 at a frequency of 500.13 MHz on a Bruker AVANCE III 500 MHz NMR spectrometer. Mass spectroscopy data were collected using ESI positive ion mode with a Thermo Scientific (San Diego, CA, USA) Q Exactive high resolution quadrupole mass spectrometer, as approximately 10 ppm solutions in 50:50 methanol: 0.1% aqueous formic acid.

2.2. Synthesis and Crystallization

The synthesis of 4-bromo-*N*-[4-hydroxy-3,5-dimethoxybenzylidene]aniline, **I**, is given as an example. A mixture of 1.722 g (10.01 mmol) 4-bromoaniline and 1.824 g (10.01 mmol) 3,5-dimethoxy-4-hydroxybenzaldehyde was refluxed for 40 min in 30 mL of absolute ethanol. The mixture was cooled to room temperature and left at -4 °C overnight to precipitate. The precipitate that formed was filtered, washed with diethyl ether, and allowed to dry, yielding 2.291 g (68.06%) as a tan solid. Single crystals of **Ia** and **Ib** suitable for X-ray diffraction were grown via the solvent diffusion of hexanes into an acetone solution of the compound. MP: 153–154 °C. IR: 1619 cm^{-1} (C=N). ^1H NMR (DMSO- d_6): δ 9.16 (br s, 1H, OH); 8.44 (s, 1H, CH=N); 7.55 (d, 2H, H_{Ar} , $J = 8.7$ Hz); 7.23 (s, 2H, H_{Ar}); 7.17 (d, 2H, H_{Ar} , $J = 8.7$ Hz); 3.83 ppm (s, 6H, OCH₃). ESI-HRMS, $\text{C}_{15}\text{H}_{14}\text{BrNO}_3$: m/z calc (found), intensity: $[\text{M} + \text{H}]^+$ 336.0236 (336.0238), 100%; 338.0215 (338.0216), 99%.

Similarly, 4-methoxy-*N*-[4-hydroxy-3,5-dimethoxybenzylidene]aniline, **II**, was prepared from 1.249 g (10.14 mmol) *p*-anisidine and 1.831 g (10.10 mmol) syringaldehyde, yielding 2.471 g (85.15%) as a white solid. Single crystals of **II** were grown via the evaporation of an acetone solution of the compound. MP: 163–164 °C. IR: 1620 cm^{-1} (C=N). ^1H NMR (DMSO- d_6): δ 9.02 (br s, 1H, OH); 8.46 (s, 1H, CH=N); 7.23 (d, 2H, H_{Ar} , $J = 8.9$ Hz); 7.21 (s, 2H, H_{Ar}); 6.96 (d, 2H, H_{Ar} , $J = 8.9$ Hz); 3.83 ppm (s, 6H, OCH₃); 3.77 ppm (s, 3H, OCH₃). ESI-HRMS, $\text{C}_{16}\text{H}_{17}\text{NO}_4$: m/z calc (found), intensity: $[\text{M} + \text{H}]^+$ 288.1236 (288.1245), 100%.

4-Hydroxy-*N*-[4-hydroxy-3,5-dimethoxybenzylidene]aniline, **III**, was prepared from 1.010 g (10.05 mmol) *p*-aminophenol and 1.857 g (10.12 mmol) syringaldehyde, yielding 1.6794 g (61.16%) as a brown solid. Single crystals of **III** were grown via the solvent diffusion of hexanes into a THF solution of the compound. MP: 222–223 °C. IR: 1620 cm^{-1} (C=N). ^1H NMR (DMSO- d_6): δ 9.38 (br s, 1H, OH); 8.95 (br s, 1H, OH); 8.42 (s, 1H, CH=N); 7.18 (s, 2H, H_{Ar}); 7.12 (d, 2H, H_{Ar} , $J = 8.8$ Hz); 6.78 (d, 2H, H_{Ar} , $J = 8.8$ Hz); 3.83 ppm (s, 6H, OCH₃). ESI-HRMS, $\text{C}_{15}\text{H}_{15}\text{NO}_4$: m/z calc (found), intensity: $[\text{M} + \text{H}]^+$ 274.1080 (274.1098).

2.3. Data Collection and Refinement

The data were collected with a Bruker APEX II CCD diffractometer at 100 (2) K using MoK α radiation ($\lambda = 0.71073 \text{ \AA}$). The data were processed and corrected for absorption using the Bruker SAINT+ software package version 2015, which includes SADABS for absorption correction [26]. The structures were solved using direct methods using SHELXS-2017, and the data were refined using SHELXL-2017 [27]. All non-H atoms were refined anisotropically. Hydrogen atoms attached to carbon were assigned positions based on the geometries of their attached carbons. Hydrogen atoms bonded to oxygen and nitrogen were assigned positions based on the Fourier difference map. See Table 1 for the final refinement parameters. The figures were made using ORTEP3 [28], Mercury [29], and CrystalExplorer [30].

Table 1. Data collection parameters.

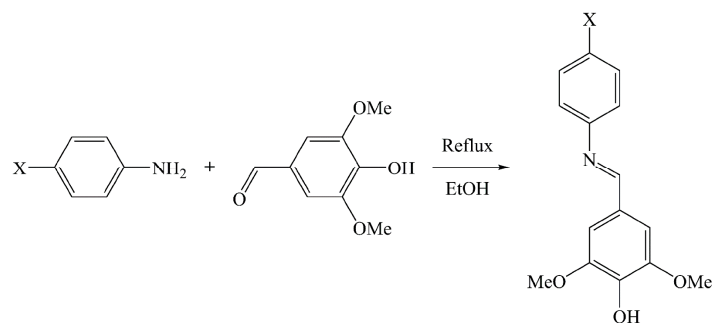
Compound	Ia (Br-m)	Ib (Br-h)	II (OMe)	III (OH)
CCDC Deposit No.	2277669	2320930	2277668	2277671
Chemical formula	C ₁₅ H ₁₄ BrNO ₃	C ₁₅ H ₁₄ BrNO ₃	C ₁₆ H ₁₇ NO ₄	C ₁₅ H ₁₅ NO ₄
M_r	336.18	336.18	287.30	273.28
Crystal system, space group	Monoclinic, $P2_1/c$	Trigonal, $R\bar{3}$	Monoclinic, $P2_1/c$	Monoclinic, $P2_1$
Temperature (K)	100 (2)	100 (2)	100 (2)	100 (2)
a, b, c (Å)	13.3573 (3) 13.7075 (3) 15.6427 (4)	27.7665 (6) 27.7665 (6) 9.6043 (3)	10.4238 (10) 12.4291 (12) 13.1323 (13)	6.1284 (5) 11.5549 (9) 9.6717 (7)
α, β, γ (°)	90 100.440 (1) 90	90 90 120	90 122.2470 (10) 90	90 98.233 (4) 90
V (Å ³)	2816.69 (11)	6412.7 (3)	1439.0 (2)	677.82 (9)
Z	8	18	4	2
Radiation type	Mo K_α	Mo K_α	Mo K_α	Mo K_α
μ (mm ⁻¹)	2.925	2.891	0.096	0.098
Crystal size (mm)	0.22 × 0.16 × 0.12	0.50 × 0.04 × 0.04	0.33 × 0.26 × 0.18	0.14 × 0.10 × 0.08
Diffractometer	Bruker APEX-II CCD			
Absorption correction	Multi-scan SADABS			
T_{\min}, T_{\max}	0.59, 0.72	0.67, 0.89	0.95, 0.98	0.95, 0.99
No. of measured, independent, and observed [$I > 2\sigma(I)$] reflections	71,268, 5987, 5627	40,757, 2832, 2633	21,013, 3053, 2826	19,802, 2938, 2855
R_{int}	0.0194	0.0251	0.0174	0.0244
$(\sin \theta / \lambda)_{\text{max}}$ (Å ⁻¹)	0.634	0.619	0.632	0.638
$R[F^2 > 2\sigma(F^2)], wR(F^2), S$	0.0205, 0.0558, 1.081	0.0188, 0.0487, 1.047	0.0323, 0.0863, 1.034	0.0256, 0.0653, 1.047
No. of reflections	5987	2832	3053	2938
No. of parameters	369	185	194	189
H-atom treatment	H atoms treated by a mixture of independent and constrained refinement			
$\Delta\rho_{\text{max}}, \Delta\rho_{\text{min}}$ (e Å ⁻³)	0.882, -0.892	0.464, -0.179	0.273, -0.205	0.190, -0.180

Computer programs: Bruker APEX2, Bruker SAINT, SHELXS97 [27], SHELXL97 [27], ORTEP-3 for Windows [28], and WinGX publication routines [28].

3. Results and Discussion

3.1. Synthesis and Spectroscopic Characterization

The compounds were synthesized by refluxing equimolar mixtures of syringaldehyde and *para*-substituted aniline in ethanol (Scheme 1). The bromo and methoxy compounds precipitated upon the cooling of the solutions, while the volume of the hydroxy complex solution had to be reduced in volume to induce precipitation. All the three compounds have bands for the C=N stretch with very similar infrared frequencies. The ¹H NMR spectra are all remarkably similar, with the common groups all having signals with similar chemical shifts. The diagnostic imine CH peak for all three compounds is at approximately 8.40 ppm, and the syringaldehyde methoxy peak is at 3.83 ppm for all of the compounds (copies of the IR, ¹H NMR, and HRMS spectra for all of the compounds can be found in Supplementary Material).



Scheme 1. The compounds were synthesized by refluxing equimolar mixtures of syringaldehyde and *para*-substituted aniline in ethanol.

3.2. Crystal Structures

Figures 1–4 are ORTEP plots of each of the structures. The bond distances and angles are mostly similar in all of the molecules (Tables 2 and 3) and similar to those of the other Schiff base molecules [30,31]. Structure **Ia** has two independent molecules in the asymmetric unit ($Z' = 2$), while the other three all have $Z' = 1$. All the molecules have the imine in the *trans* configuration, which is common for diarylimines [23,31–33], and they all have the 3,5-methoxy groups, with their methyl groups oriented towards the imine end of the molecule rather than towards the hydroxy end. This is likely to create more space for the hydroxy group to participate in intermolecular O–H···N hydrogen bonding. In fact, other than the orientation of the C17–O17–H17 bond in **Ib**, the syringaldehyde ends of the molecules are remarkably similar (Figure 5). The second aromatic rings from the aniline molecule in the synthesis have a variety of orientations (Figure 6), likely due to the packing efficiency needs. In structure **Ia**, the only major difference in the two independent molecules is the rotation of the C1–C6 benzene ring relative to the C9–C14 ring (Figure 7).

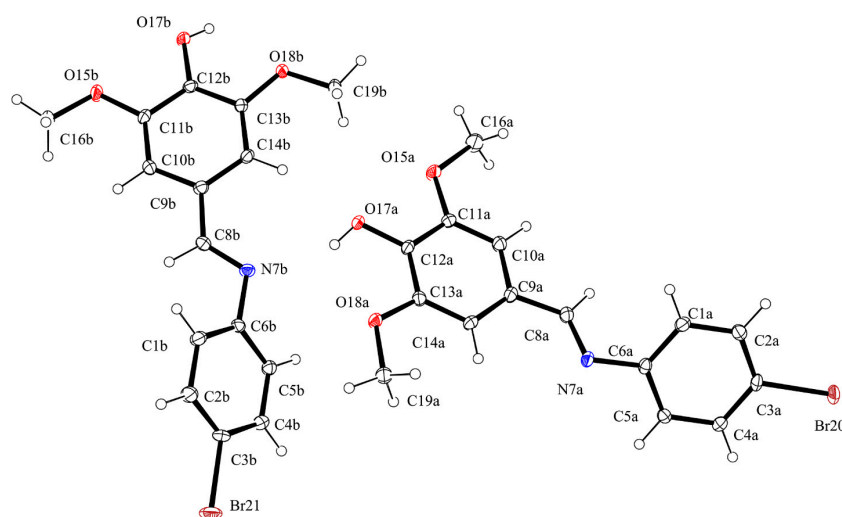


Figure 1. ORTEP diagram of compound **Ia** with thermal ellipsoids shown at the 50% probability level and hydrogen atoms as spheres of arbitrary size.

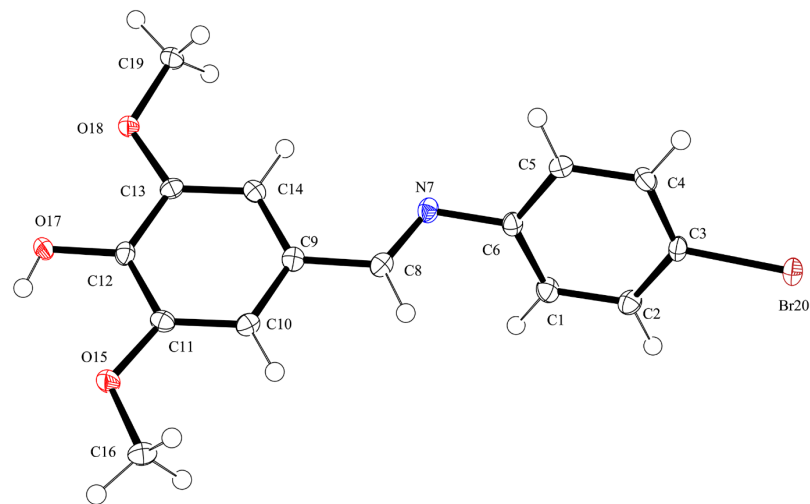


Figure 2. ORTEP diagram of compound **Ib** with thermal ellipsoids shown at the 50% probability level and hydrogen atoms as spheres of arbitrary size.

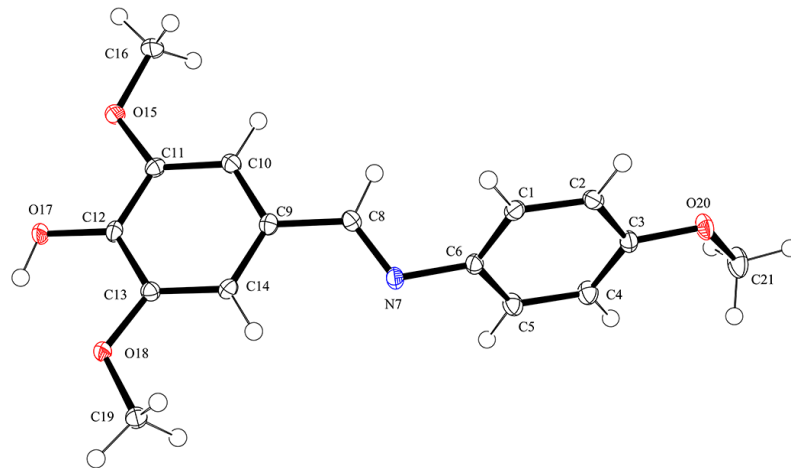


Figure 3. ORTEP diagram of compound **II** with thermal ellipsoids shown at the 50% probability level and hydrogen atoms as spheres of arbitrary size.

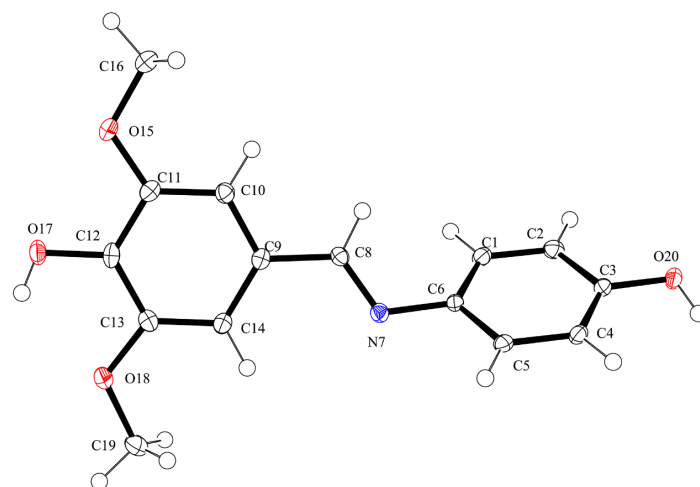


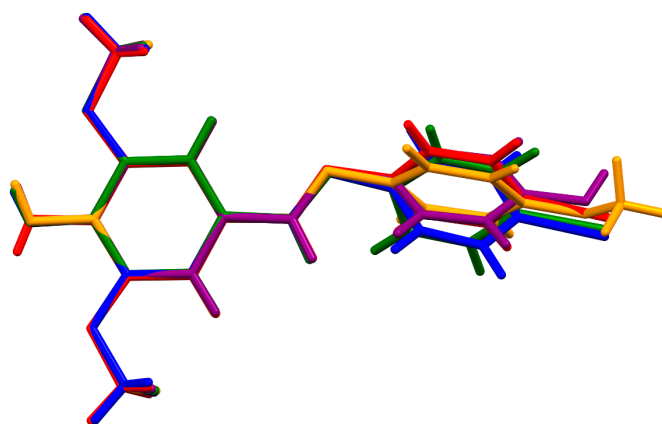
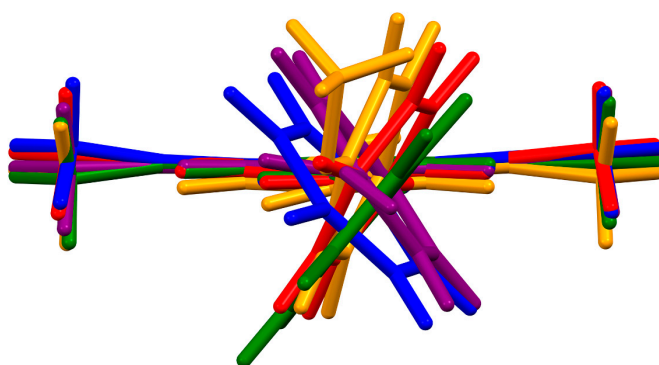
Figure 4. ORTEP diagram of compound **III** with thermal ellipsoids shown at the 50% probability level and hydrogen atoms as spheres of arbitrary size.

Table 2. Selected bond distances (Å).

Bond	Ia	Ib	II	III
C6–N7	1.4262 (18), 1.4222 (18)	1.4265 (19)	1.4325 (13)	1.4278 (19)
N7–C8	1.2852 (19), 1.2840 (19)	1.281 (2)	1.2828 (13)	1.283 (2)
C8–C9	1.4633 (19), 1.4566 (19)	1.464 (2)	1.4678 (13)	1.468 (2)
C12–O17	1.3611 (17), 1.3529 (17)	1.3554 (18)	1.3609 (12)	1.363 (2)

Table 3. Selected bond angles (°).

Bond	Ia	Ib	II	III
C6–N7–C8	115.68 (12), 114.79 (12)	116.88 (13)	116.16 (9)	117.50 (13)
N7–C8–C9	126.63 (13), 126.20 (13)	124.55 (14)	124.51 (9)	123.26 (14)
C11–O15–C16	116.99 (12), 116.55 (11)	116.80 (12)	116.82 (8)	116.73 (13)
C12–O17–H17	110.9 (15), 112.5 (17)	110.0 (17)	112.1 (12)	108.5 (18)
C13–O18–C19	116.51 (11), 166.31 (11)	116.76 (12)	116.57 (8)	117.04 (13)

**Figure 5.** Capped stick overlay of all molecules, showing the similarities in the syringaldehyde end of the imines. Molecule **IaA** is shown in green; **IaB** is shown in blue; **Ib** is shown in red; **II** is shown in yellow; and **III** is shown in purple.**Figure 6.** Capped stick overlay of all molecules, looking along the imine bond from the aniline end of the molecules, showing the different rotations of the aniline moieties relative to the syringaldehyde moieties. Molecule **IaA** is shown in green; **IaB** is shown in blue; **Ib** is shown in red; **II** is shown in yellow; and **III** is shown in purple.

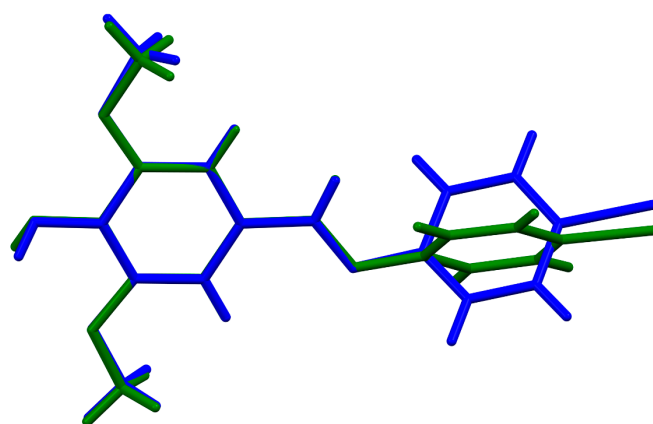


Figure 7. Capped stick overlay of the two independent molecules in structure **Ia**. Molecule **IaA** is shown in green, and **IaB** is shown in blue.

Structures **Ia**, **II**, and **III** crystallize in monoclinic space groups, and the molecules form zigzag chains via the O–H···N hydrogen bonds (Figures 8–10 and Tables 4–6). In structures **Ia** and **II**, the syringaldehyde O–H is involved in intermolecular hydrogen bonding, while in **III**, the syringaldehyde hydroxy is primarily involved in an intramolecular hydrogen bond with methoxy oxygen; however, the intermolecular O–H···N hydrogen bonds involve the less sterically hindered hydroxy group from the aniline end of the molecule (Figure 10). In all the three structures, the syringaldehyde O–H is orientated *cis* to the imine N=C bond, resulting in the zigzag chains structures of **Ia** along *a* and **II** along *c*. However, in structure **Ib**, the hydroxy group is orientated *trans* to the imine N=C bond, resulting in a hexagonal structure composed of rings containing six imine molecules held together with O–H···N hydrogen bonds (Figure 11 and Table 7).

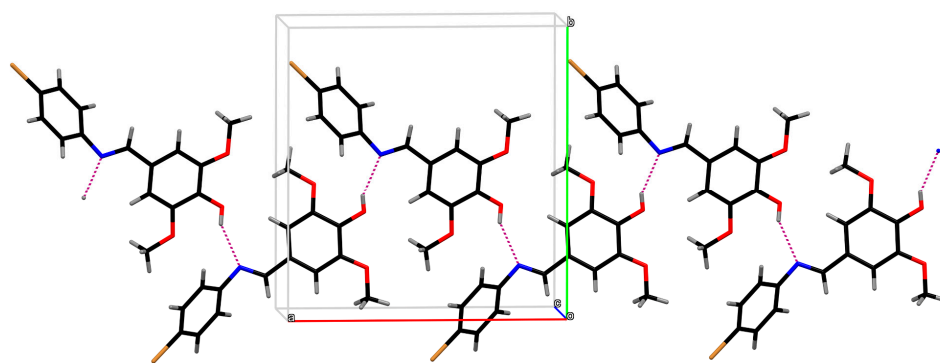


Figure 8. Hydrogen-bonded chains in **Ia**.

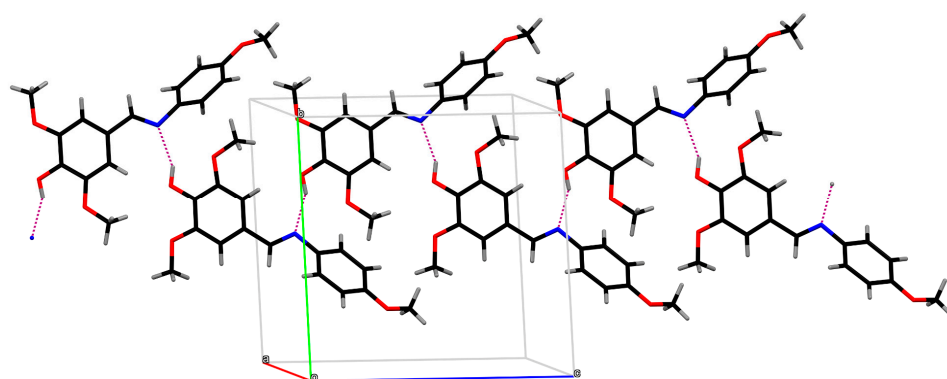


Figure 9. Hydrogen-bonded chains in **II**.

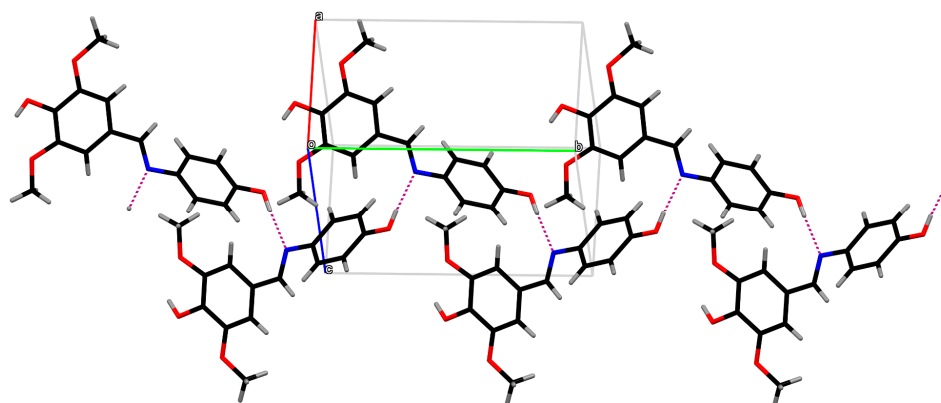


Figure 10. Hydrogen-bonded chains in III.

Table 4. Parameters (\AA , $^\circ$) for hydrogen bonds and contacts in compound Ia.

$D-H \cdots A$	$D-H$	$H \cdots A$	$D \cdots A$	$D-H \cdots A$
C14A–H14A \cdots O17B ⁱ	0.95	2.26	3.1771 (17)	163
C2A–H2A \cdots O17A ⁱⁱ	0.95	2.60	3.3113 (18)	133
O17A–H17A \cdots N7B	0.80 (2)	2.22 (2)	2.9442 (16)	151.7 (19)
C14B–H14B \cdots O17A	0.95	2.36	3.2847 (17)	166
C1B–H1B \cdots O18B ⁱⁱⁱ	0.95	2.55	3.4854 (18)	169
C2B–H2B \cdots O17B ⁱⁱⁱ	0.95	2.53	3.2262 (19)	130
C4B–H4B \cdots Br21 ^{iv}	0.95	2.88	3.7816 (15)	160
O17B–H17B \cdots N7A ^v	0.76 (2)	2.17 (2)	2.8553 (17)	152 (2)

Symmetry codes: (i) $x + 1, y, z$; (ii) $-x + 1, y + 1/2, -z + 1/2$; (iii) $-x, y - 1/2, -z + 1/2$; (iv) $-x + 1, -y, -z$; (v) $x - 1, y, z$.

Table 5. Parameters (\AA , $^\circ$) for hydrogen bonds and contacts in compound II.

$D-H \cdots A$	$D-H$	$H \cdots A$	$D \cdots A$	$D-H \cdots A$
C14–H14 \cdots O17 ⁱ	0.95	2.24	3.1680 (12)	165
C8–H8 \cdots O20 ⁱⁱ	0.95	2.60	3.3906 (13)	141
C1–H1 \cdots O18 ⁱⁱⁱ	0.95	2.57	3.5027 (13)	166
C19–H19B \cdots O15 ⁱ	0.98	2.65	3.1313 (13)	110
O17–H17 \cdots N7 ^{iv}	0.87 (2)	2.10 (2)	2.9010 (12)	152.5 (17)

Symmetry codes: (i) $x, -y + 3/2, z + 1/2$; (ii) $x, -y + 5/2, z - 1/2$; (iii) $-x, y + 1/2, -z + 1/2$; (iv) $x, -y + 3/2, z - 1/2$.

Table 6. Parameters (\AA , $^\circ$) for hydrogen bonds and contacts in compound III.

$D-H \cdots A$	$D-H$	$H \cdots A$	$D \cdots A$	$D-H \cdots A$
C10–H10 \cdots O17 ⁱ	0.95	2.36	3.271 (2)	160
O20–H20 \cdots N7 ⁱⁱ	0.85 (3)	1.92 (3)	2.7693 (19)	176 (3)
O17–H17 \cdots N7 ⁱⁱⁱ	0.81 (3)	2.54 (3)	3.0061 (18)	117 (2)
O17–H17 \cdots O18	0.81 (3)	2.21 (2)	2.6432 (18)	114 (2)

Symmetry codes: (i) $-x + 1, y + 1/2, -z$; (ii) $-x, y + 1/2, -z + 1$; (iii) $-x, y - 1/2, -z$.

Table 7. Parameters (\AA , $^\circ$) for hydrogen bonds and contacts in compound Ib.

$D-H \cdots A$	$D-H$	$H \cdots A$	$D \cdots A$	$D-H \cdots A$
C14–H14 \cdots O17 ⁱ	0.95	2.29	3.1785 (18)	156
C19–H19 \cdots O18 ⁱ	0.98	2.52	3.1870 (19)	125
O17–H17 \cdots N7 ⁱⁱ	0.75 (2)	2.21 (2)	2.8819 (17)	150 (2)
O17–H17 \cdots O15	0.75 (2)	2.28 (2)	2.6659 (15)	113 (2)

Symmetry codes: (i) $x - y + 2/3, x + 1/3, -z + 4/3$; (ii) $y - 1/3, -x + y + 1/3, -z + 4/3$.

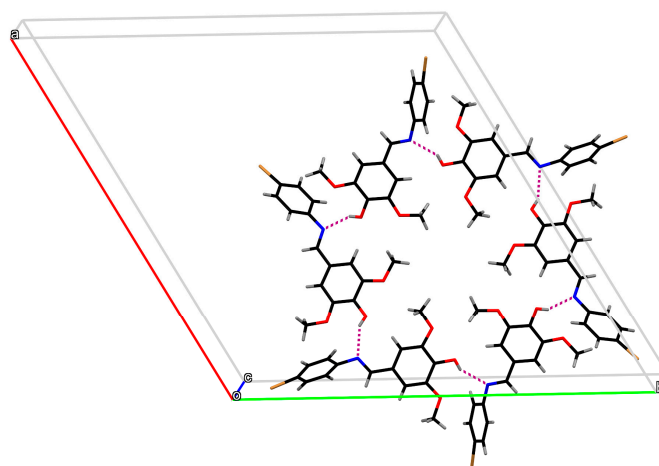


Figure 11. Hydrogen-bonded rings in **1b**.

3.3. Hirshfeld Analysis

Upon examination of the Hirshfeld surface plots for all five molecules (Figures 12–16), several similarities are evident. In all five molecules, the imine nitrogen (N7) is a strong hydrogen bond acceptor, as indicated by the deep red spot on the surface plot near the atom. Syringaldehyde hydroxy hydrogen (H17) is the hydrogen bond donor to N7 in all but molecule **III**, as evidenced by the red spots near H17 in the surface plots. Interestingly, the syringaldehyde hydroxy group of molecule **III** is not involved in any strong intermolecular hydrogen bonding interactions; the other hydroxy group is much less sterically hindered, allowing it to preferentially hydrogen bond with the imine nitrogen N7 in **III**. Several of the structures also show close contact between H10 and O17, which can be seen on the Hirshfeld surface plots.

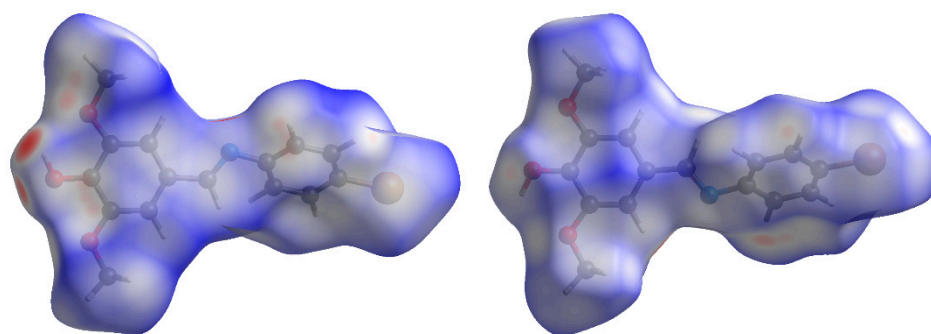


Figure 12. Hirshfeld surface of the A molecule of **Ia**, showing two faces of the molecule.

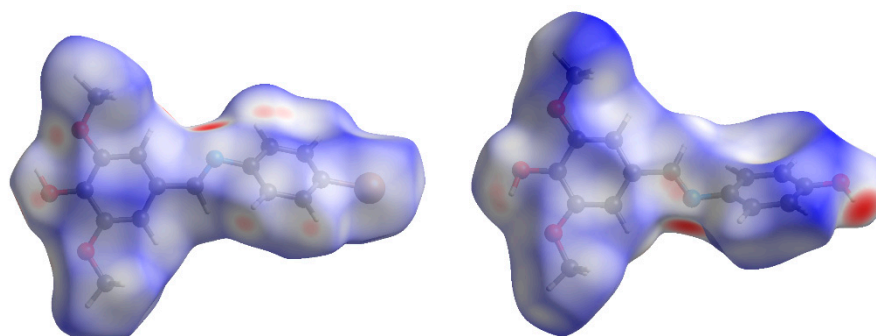


Figure 13. Hirshfeld surface of the B molecule of **Ia**, showing two faces of the molecule.

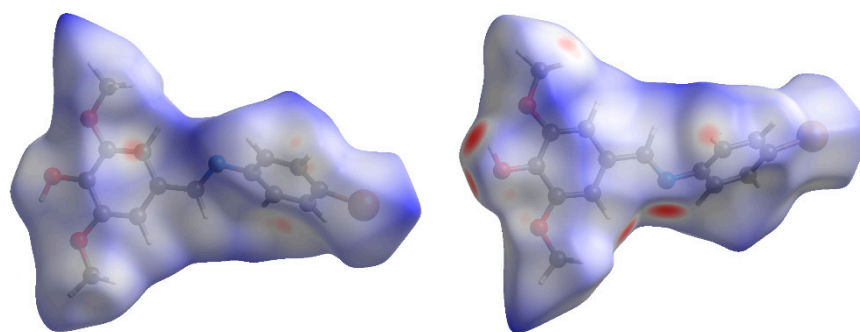


Figure 14. Hirshfeld surface of the molecule of **Ib**, showing two faces of the molecule.

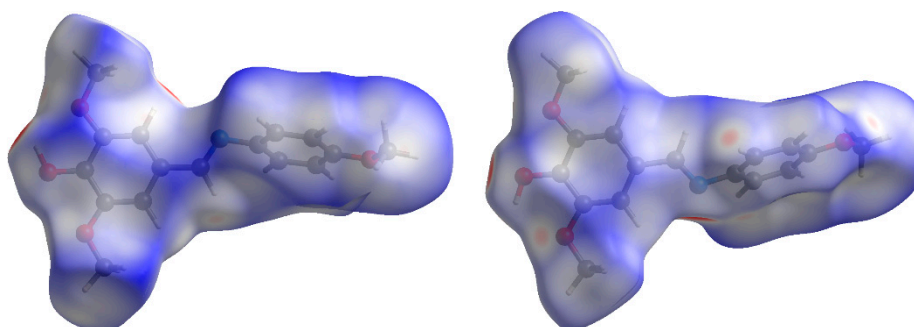


Figure 15. Hirshfeld surface of the molecule of **II**, showing two faces of the molecule.

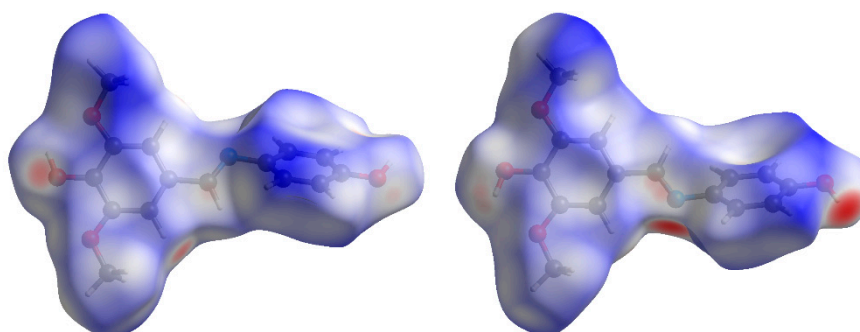


Figure 16. Hirshfeld surface of the molecule of **III**, showing two faces of the molecule.

For all five molecules, the most common form of intermolecular contact, by percentage of the surfaces, is with $H \cdots H$, followed by $C \cdots H/H \cdots C$. For all but molecule **Ia-B**, $O \cdots H/H \cdots O$ contact is the third most common, while it is the fourth most common in **Ia-B**, which is slightly behind $Br \cdots H/H \cdots Br$ (Figure 17). For molecules **Ia** and **Ib**, $O \cdots H/H \cdots O$ and $Br \cdots H/H \cdots Br$ contact make up similar proportions of the totals. For all of the molecules, $N \cdots H/H \cdots N$ contact is the fourth most common non-bromine interaction, but it is the closest, and presumably strongest, form of contact in all of the structures. Interestingly, for the bromine-substituted compounds (**Ia** and **Ib**), only **Ib** has any $Br \cdots Br$ contacts (3.9%), while the **Ia** molecules have a small number of $Br \cdots C/C \cdots Br$ contact points. The bromine atoms are on the outside of the hexamers in **Ib** (Figure 11), while the bromine atoms in structure **Ia** are less exposed (Figure 8). Additionally, there are very few $C \cdots C$ contact points (highest is 3.1% in **Ia-A**), and there is no evidence of strong π - π interactions.

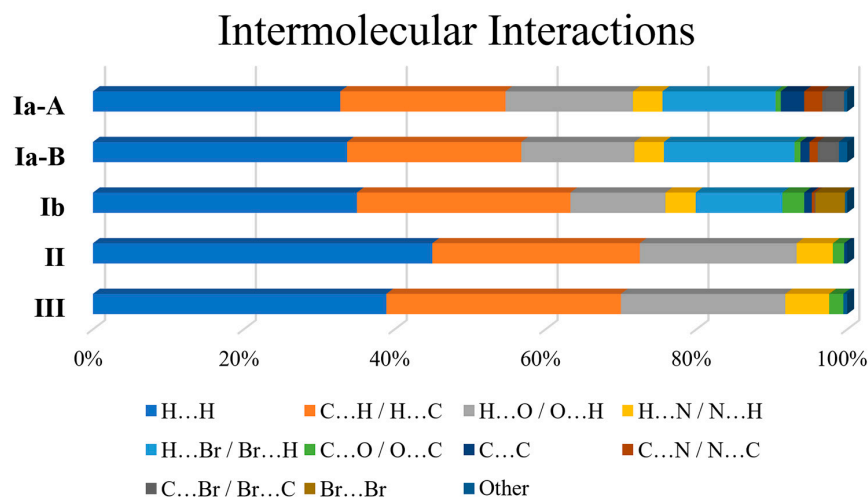


Figure 17. Graph showing contributions of intermolecular interactions in the molecules.

Looking more closely at the $\text{Br}\cdots\text{Br}$ contact points in **Ib**, there are hexamers of **Ib** molecules (Figure 18) held together by very weak halogen bond interactions, with $\text{Br}\cdots\text{Br}$ distances of 3.9450(3) Å. While this distance is longer than the sum of the commonly accepted Bondi van der Waals radii [34], it is within the sum of van der Waals radii as determined by Chernyshov (2.00 Å) [35]. These weak halogen bond interactions account for the 3.9% of $\text{Br}\cdots\text{Br}$ contact points in **Ib**.

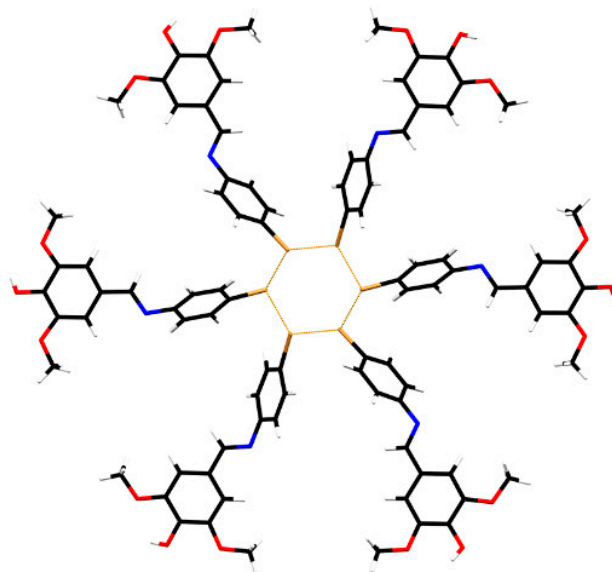


Figure 18. Rings of molecules in **Ib** formed by $\text{Br}\cdots\text{Br}$ interactions.

All five molecules have similar fingerprint plots (Figures 19–23). All of the fingerprint plots show sharp “fangs” corresponding to $\text{O}\cdots\text{H}\cdots\text{O}$ (Figures 19d, 20d, 21d, 22d and 23d) and $\text{O}\cdots\text{H}\cdots\text{N}$ (Figures 19c, 20c, 21c, 22c and 23c) hydrogen bonds, as indicated on the plots. While all of the structures show shorter $\text{O}\cdots\text{H}\cdots\text{N}$ interactions compared to the $\text{O}\cdots\text{H}\cdots\text{O}$ interactions, in molecule III, the $\text{O}\cdots\text{H}\cdots\text{N}$ interaction is significantly shorter than those in the other four molecules. This is likely due to the decrease steric hindrance of the aniline *para*-hydroxy group compared to the syringaldehyde hydroxy groups that are the imine nitrogen hydrogen-bonding partners in the other four molecules. The decreased steric hindrance allows for a shorter, and presumably stronger, interaction compared to that of the syringaldehyde hydroxy group.

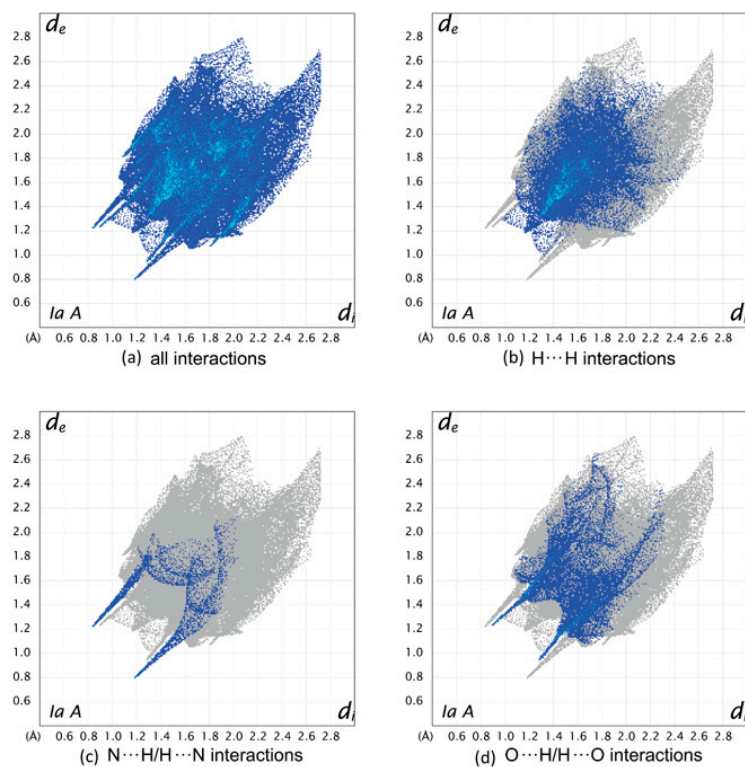


Figure 19. Fingerprint plots for the A molecule of **Ia**; (a) all interactions, (b) H···H interactions, (c) N···H/H···N interactions, and (d) O···H/H···O interactions.

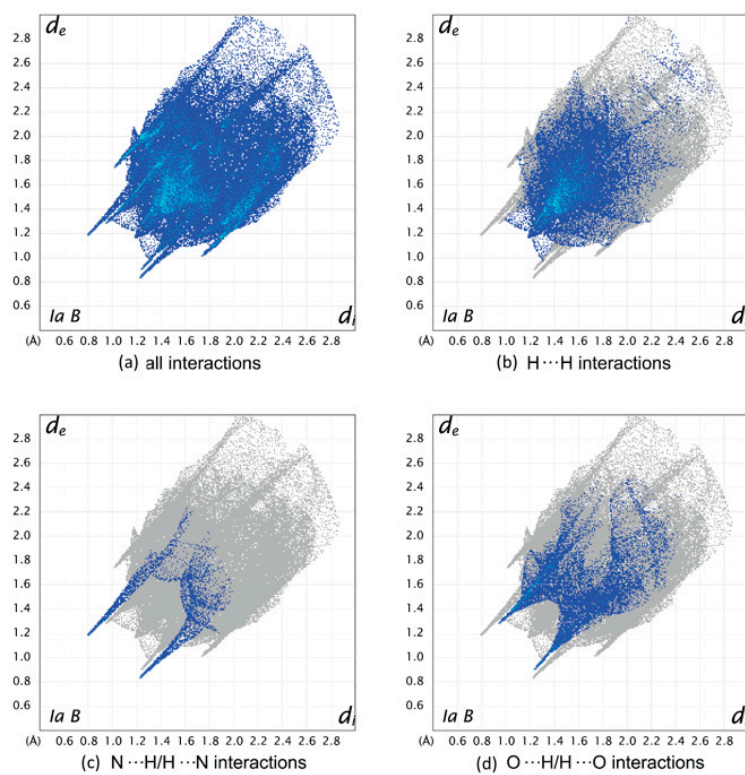


Figure 20. Fingerprint plot of the B molecule of **Ia**; (a) all interactions, (b) H···H interactions, (c) N···H/H···N interactions, and (d) O···H/H···O interactions.

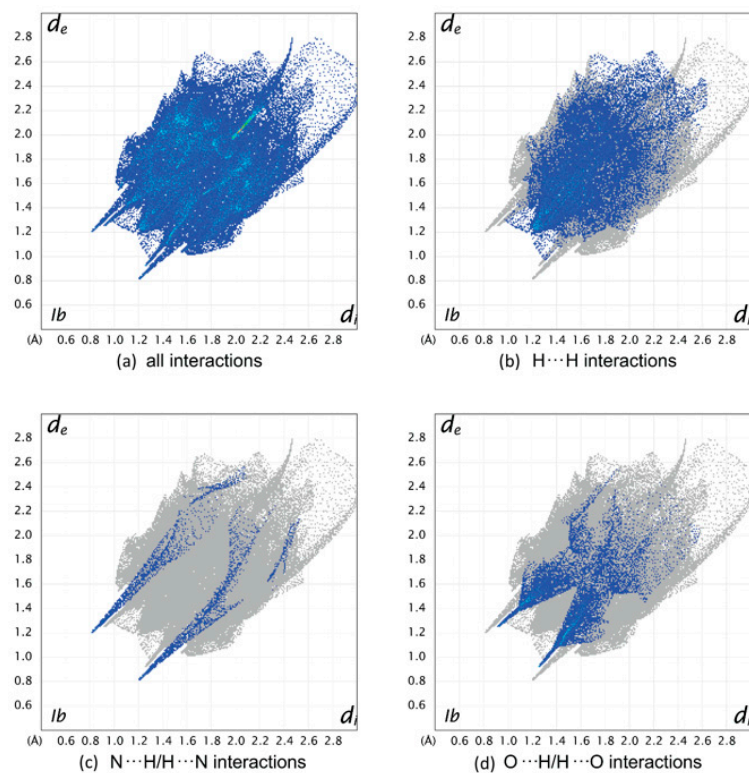


Figure 21. Fingerprint plot of Ib (a) all interactions, (b) H...H interactions, (c) N...H/H...N interactions, and (d) O...H/H...O interactions.

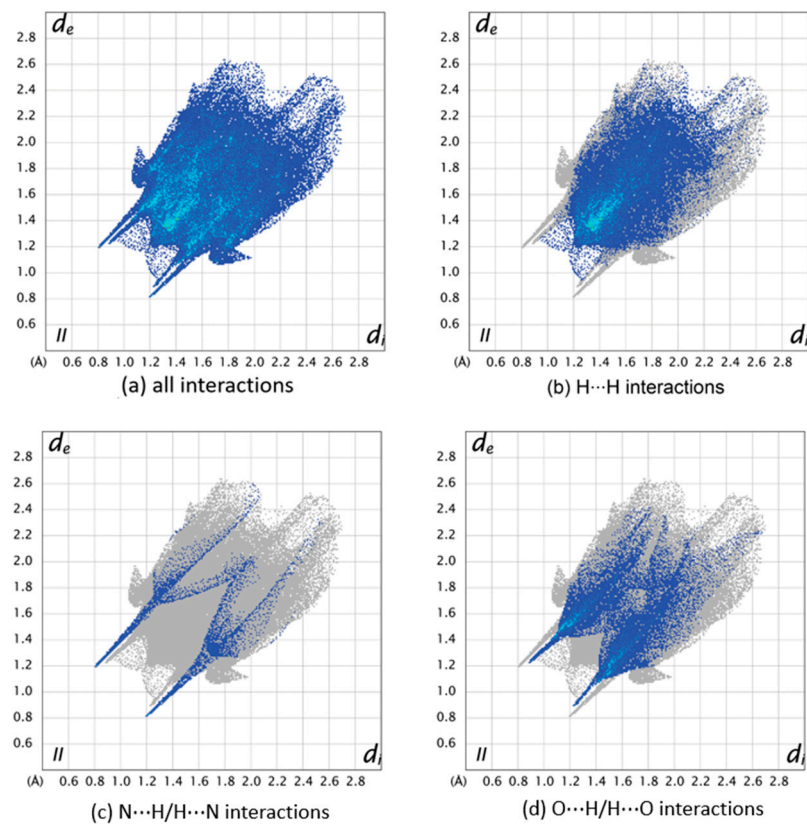


Figure 22. Fingerprint plot of II (a) all interactions, (b) H...H interactions, (c) N...H/H...N interactions, and (d) O...H/H...O interactions.

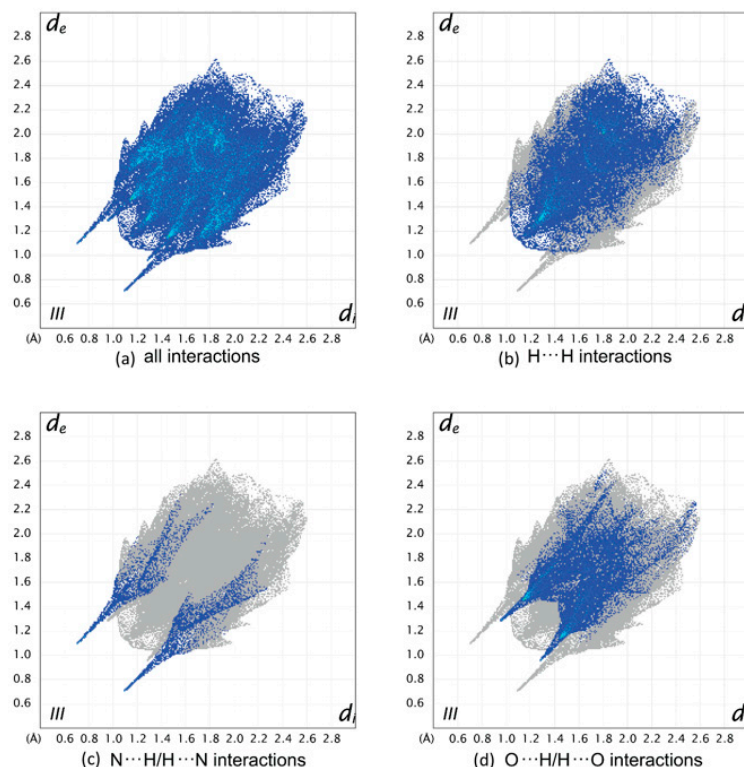


Figure 23. Fingerprint plot of **III** (a) all interactions, (b) $\text{H}\cdots\text{H}$ interactions, (c) $\text{N}\cdots\text{H}/\text{H}\cdots\text{N}$ interactions, and (d) $\text{O}\cdots\text{H}/\text{H}\cdots\text{O}$ interactions.

3.4. Hydrogen Bonding Analysis

A Cambridge Structural Database search for *p*-hydroxyphenyl imine structures reveals similar patterns in intermolecular $\text{O}\cdots\text{H}\cdots\text{N}$ hydrogen bonding (search using CCDC ConQuest Version 2023.3.0. Only structures with no disorder and R values less than 10 were considered. If more than one structure of a molecule was published, the reference at the lowest temperature was used). For 40 structures (47 measurements) with two hydrogen atoms *ortho* to the hydrogen-bonding hydroxyl group, the average $\text{O}\cdots\text{N}$ contact distance was $2.773 \pm 0.051 \text{ \AA}$, with a range of 2.687 \AA – 2.902 \AA , which is very similar to the $\text{O}20\cdots\text{N}7$ contact distance in **III** ($2.7693 (19) \text{ \AA}$). When the search was conducted for structures with one hydrogen atom and one non-hydrogen atom *ortho* to the hydroxyl group, the average $\text{O}\cdots\text{N}$ contact distance was $2.843 \pm 0.056 \text{ \AA}$, with a range of 2.775 \AA – 2.979 \AA , for 15 structures with 21 measured hydrogen-bonding interactions. While the measurements are within the margin of error of each other, the general trend with the average and range is a slight lengthening of the interaction. When the search was conducted for structures with two non-hydrogen groups in the *ortho* positions, only four structures (with five measurements) were identified, with an average $\text{O}\cdots\text{N}$ contact distance of $2.882 \pm 0.062 \text{ \AA}$ and with a range of 2.802 \AA – 2.941 \AA , which makes it the longest of the three types of structure. The $\text{O}\cdots\text{N}$ distances in the reported structures are $2.9442 (16) \text{ \AA}$ and $2.8553 (17) \text{ \AA}$ for **Ia**, $2.8819 (17) \text{ \AA}$ for **Ib**, and $2.9010 (12) \text{ \AA}$ for **II**. The average $\text{O}\cdots\text{N}$ contact distance in **Ia**, **Ib**, and **II** is $2.896 \pm 0.037 \text{ \AA}$, which is very similar to that of the previously reported structures. Again, while the distances are statistically similar, the general trend is for longer hydrogen-bonding distances as the steric hinderance around the hydroxyl group increases.

4. Conclusions

The orientation of the syringaldehyde hydroxyl group relative to the $\text{C}=\text{N}=\text{C}-\text{C}$ imine group plays a major role in the pattern of hydrogen bonding in syringaldehyde imine molecules. The three crystal structures presented here with *cis*-syringaldehyde hydroxy groups positioned relative to $\text{C}=\text{N}=\text{C}-\text{C}$ imine give rise to hydrogen-bonded zigzag chains

of molecules. The example with a *trans*-syringaldehyde hydroxy group positioned relative to C=N=C-C imine crystalized in a hexagonal space group with six-membered rings formed by the O–H···N hydrogen bonds. While O–H···N hydrogen bonding interactions make up a relatively small percentage of the intermolecular contact types in the crystal structures, they are the major driving force for the three dimensional packing of the molecules in their crystals. We continue to investigate the factors that give rise to the *cis*- vs. *trans*- orientation of the *p*-hydroxyl group in hopes of a better understanding of crystal packing and crystal structure prediction.

Supplementary Materials: The following supporting information can be downloaded at: <https://www.mdpi.com/article/10.3390/cryst14010099/s1>, S1: copies of the IR, ¹H NMR, and HRMS spectra for all of the compounds. CCDC 2277668–2277671 contain the supplementary crystallographic data for this paper. These data can be obtained free of charge from the Cambridge Crystallographic Data Centre via www.ccdc.cam.ac.uk/structures (accessed on 27 December 2023).

Author Contributions: Methodology and investigation, S.M.G. and C.G.H.; preliminary writing, S.M.G.; writing—review and editing, C.G.H.; supervision and funding acquisition, C.G.H. All authors have read and agreed to the published version of the manuscript.

Funding: C.G.H. thanks the Illinois State University Chemistry Department for financial support. We also thank the NSF (grant No. CHE-1039689) for funding the X-ray diffractometer.

Data Availability Statement: The original contributions presented in the study are included in the article/supplementary material, further inquiries can be directed to the corresponding author.

Conflicts of Interest: The authors declare no conflicts of interest.

References

1. Schiff, H. Mittheilungen aus dem Universitätslaboratorium in Pisa: Eine neue Reihe organischer Basen. *Leibigs Ann. Chem.* **1864**, *131*, 118–119. [[CrossRef](#)]
2. Hamaker, C.G.; Halbach, D.P. Synthesis, structure, and characterization of some ruthenium arene complexes of *N*-(arylmethylene)-2-(methylthio)anilines and 2-(methylthio)aniline. *Inorg. Chim. Acta* **2006**, *359*, 846–853. [[CrossRef](#)]
3. Pervaiz, M.; Sadiq, S.; Sadiq, A.; Younas, U.; Ashraf, A.; Saeed, Z.; Zuber, M.; Adnan, A. Azo-Schiff base derivatives of transition metal complexes as antimicrobial agents. *Coord. Chem. Rev.* **2021**, *447*, 214128. [[CrossRef](#)]
4. Gonul, I.; Demirbag, B.; Ocakoglu, K.; Ayaz, F. Unique photodynamic antimicrobial Schiff bases and their copper complexes exert immunomodulatory activity on mammalian macrophages. *J. Coord. Chem.* **2020**, *73*, 2878–2888. [[CrossRef](#)]
5. Sun, Y.; Lu, Y.; Bian, M.; Yang, Z.; Ma, X.; Liu, W. Pt(II) and Au(III) complexes containing Schiff-base ligands: A promising source for antitumor treatment. *Eur. J. Med. Chem.* **2021**, *211*, 113098. [[CrossRef](#)]
6. Padnya, P.; Shibaeva, K.; Arsenyev, M.; Baryshnikova, S.; Tereteva, O.; Shiabiev, I.; Khannanov, A.; Boldyrev, A.; Gerasimov, A.; Grishaev, D.; et al. Catechol-Containing Schiff Bases on Thiocalixarene: Synthesis, Copper (II) Recognition, and Formation of Organic-Inorganic Copper-Based Materials. *Molecules* **2021**, *26*, 2334. [[CrossRef](#)]
7. Creighton, R.H.J.; McCarthy, J.L.; Hibbert, H. Aromatic Aldehydes from Spruce and Maple Woods. *J. Am. Chem. Soc.* **1941**, *63*, 312. [[CrossRef](#)]
8. Guchu, E.; Diaz-Maroto, M.C.; Diaz-Maroto, I.J.; Vila-Lameiro, P.; Perez-Coello, M.S. Influence of the Species and Geographical Location on Volatile Composition of Spanish Oak Wood (*Quercus petraea* Liebl. and *Quercus robur* L.). *J. Agric. Food Chem.* **2006**, *54*, 3062–3066. [[CrossRef](#)]
9. Goldberg, D.M.; Hoffman, B.; Yang, J.; Soleas, G.J. Phenolic Constituents, Furans, and Total Antioxidant Status of Distilled Spirits. *J. Agric. Food Chem.* **1999**, *47*, 3978–3985. [[CrossRef](#)]
10. Alcarde, A.R.; Souza, L.M.; Bortoletto, A.M. Formation of volatile and maturation-related congeners during the aging of sugarcane spirit in oak barrels. *J. Inst. Brew.* **2014**, *120*, 529–536. [[CrossRef](#)]
11. Ibrahim, M.N.M.; Sriprasanthi, R.B.; Shamsudeen, S.; Adam, F.; Bhawani, S.A. A concise review of the natural existence, synthesis, properties, and applications of syringaldehyde. *BioResources* **2012**, *7*, 4377–4399. [[CrossRef](#)]
12. Kuo, S.C.; Chung, H.H.; Huang, C.H.; Cheng, J.T. Decrease of Hyperglycemia by Syringaldehyde in Diabetic Rats. *Horm. Metab. Res.* **2014**, *46*, 8–13. [[CrossRef](#)]
13. Huang, C.H.; Chen, M.F.; Chung, H.H.; Cheng, J.T. Antihyperglycemic Effect of Syringaldehyde in Streptozotocin-Induced Diabetic Rats. *J. Nat. Prod.* **2012**, *75*, 1465–1468. [[CrossRef](#)]
14. Shahzad, S.; Mateen, S.; Mariyath, P.M.M.; Naem, S.S.; Akhtar, K.; Rizvi, W.; Moin, S. Protective effect of syringaldehyde on biomolecular oxidation, inflammation and histopathological alterations in isoproterenol induced cardiotoxicity in rats. *Biomed. Pharmacother.* **2018**, *108*, 625–633. [[CrossRef](#)]

15. Yancheva, D.; Velcheva, E.; Glavcheva, Z.; Stamboliyska, B.; Smelcerovic, A. Insights in the radical scavenging mechanism of syringaldehyde and generation of its anion. *J. Molec. Struct.* **2016**, *1108*, 552–559. [[CrossRef](#)]
16. Stanikunaite, R.; Khan, S.I.; Trappe, J.M.; Ross, S.A. Cyclooxygenase-2 inhibitory and antioxidant compounds from the truffle *elaphomyces granulatus*. *Phytother. Res.* **2009**, *23*, 575–578. [[CrossRef](#)]
17. Aytac, S.; Gundogdu, O.; Bingol, Z.; Gulcin, I. Synthesis of Schiff Bases Containing Phenol Rings and Investigation of Their Antioxidant Capacity, Anticholinesterase, Butyrylcholinesterase, and Carbonic Anhydrase Inhibition Properties. *Pharmaceutics* **2023**, *15*, 779. [[CrossRef](#)]
18. McCrone, W.C. Polymorphism. In *Physics and Chemistry of the Organic Solid State*; Fox, D., Labes, M.M., Weissberger, A., Eds.; Interscience: New York, NY, USA, 1965; Volume 2, pp. 725–767.
19. Bernstein, J.; Davey, R.J.; Henck, J.O. Concomitant polymorphs. *Angew. Chem. Int. Ed.* **1999**, *38*, 3440–3461. [[CrossRef](#)]
20. Gong, N.; Hu, K.; Jin, G.; Du, G.; Lu, Y. Concomitant polymorphs of methoxyflavone (5-methyl-7-methoxyflavone). *RSC Adv.* **2016**, *6*, 38709–38715. [[CrossRef](#)]
21. Kuš, P.; Borek, J.; Jones, P.G. Two concomitant polymorphs of *N,N'*-bis [4-(diethylamino)phenyl]terephthaldiamide. *Acta Crystallogr. Sect. C Struct. Chem.* **2010**, *C66*, o93–o96. [[CrossRef](#)]
22. Lee, E.H. A practical guide to pharmaceutical polymorph screening & selection. *Asian J. Pharm. Sci.* **2014**, *9*, 163–175.
23. Hamaker, C.G.; Maryashina, O.S.; Daley, D.K.; Wadler, A.L. Synthesis and Crystal Structures of Two Schiff Bases of 2-(Methylthio)aniline with Halogenated Salicylaldehydes. *J. Chem. Crystallogr.* **2010**, *40*, 34–39. [[CrossRef](#)]
24. Goettler, P.E.; Hamaker, C.G. Crystal Structure Analysis of Two 4-Nitro-N-methylaniline Derivatives. *J. Chem. Crystallogr.* **2022**, *52*, 251–259. [[CrossRef](#)]
25. Li, E.W.; Katinas, J.; Jones, M.A.; Hamaker, C.G. Structural characterization of naphthalene sulfonamides and a sulfonate ester and their in vitro efficacy against *Leishmania tarentolae* promastigotes. *New J. Chem.* **2021**, *45*, 4791–4801. [[CrossRef](#)]
26. Bruker AXS Inc. *SAINT*; Bruker AXS Inc.: Madison, WI, USA, 2015.
27. Sheldrick, G.M. Crystal Structure Refinement with SHELXL. *Acta Crystallogr. Sect. C Struct. Chem.* **2015**, *C71*, 3–8. [[CrossRef](#)]
28. Farrugia, L.J. WinGX and ORTEP for Windows: An Update. *J. Appl. Crystallogr.* **2012**, *45*, 849–854. [[CrossRef](#)]
29. Macrae, C.F.; Sovago, I.; Cottrell, S.J.; Galek, P.T.A.; McCabe, P.; Pidcock, E.; Platings, M.; Shields, G.P.; Stevens, J.S.; Towler, M.; et al. Mercury 4.0: From visualization to analysis, design and prediction. *J. Appl. Crystallogr.* **2020**, *53*, 226–235. [[CrossRef](#)]
30. Turner, M.J.; McKinnon, J.J.; Wolff, S.K.; Grimwood, D.J.; Spackman, P.R.; Jayatilaka, D.; Spackman, M.A. *Crystal Explorer 17*; The University of Western Australia: Perth, Australia, 2017.
31. Hamaker, C.G.; Oberts, B.P. Synthesis and crystal structures of the bis-Schiff bases of 2-(methylthio)aniline with isophthalaldehyde, terephthalaldehyde, and *para*-diacetylbenzene. *J. Chem. Crystallogr.* **2006**, *36*, 735–742. [[CrossRef](#)]
32. Khalaji, A.D.; Asghari, J.; Fejfarová, K.; Dušek, M. 4-Chloro-*N*-(3,4,5-trimethoxybenzylidene)aniline *Acta Crystallogr. Sect. E Crystallogr. Commun.* **2009**, *E65*, o253. [[CrossRef](#)]
33. Khalaji, A.D.; Weil, M.; Gotoh, K.; Ishida, H. 4-Bromo-*N*-(3,4,5-trimethoxybenzylidene)aniline. *Acta Crystallogr. Sect. E Crystallogr. Commun.* **2009**, *E65*, o436. [[CrossRef](#)]
34. Bondi, A. Van der Waals Volumes and Radii. *J. Phys. Chem.* **1964**, *68*, 441–451. [[CrossRef](#)]
35. Chernyshov, I.Y.; Ananyev, I.V.; Pidko, E.A. Revisiting van der Waals Radii: From Comprehensive Structural Analysis to Knowledge-Based Classification of Interatomic Contacts. *ChemPhysChem* **2020**, *21*, 370–376. [[CrossRef](#)]

Disclaimer/Publisher's Note: The statements, opinions and data contained in all publications are solely those of the individual author(s) and contributor(s) and not of MDPI and/or the editor(s). MDPI and/or the editor(s) disclaim responsibility for any injury to people or property resulting from any ideas, methods, instructions or products referred to in the content.